Science for Energy and Environment
https://www.sciltp.com/journals/see

Check for updates

Article

Methanol from Catalytic Conversion of Biogas-Based Syngas (CO, H_2)

Yitong Jiang [1], Jin Zhang [1], Huili Zhang [2,*] and Jan Baeyens [1]

[1] Beijing Advanced Innovation Centre for Soft Matter Science and Engineering, Beijing University of Chemical Technology, Beijing 100029, China
[2] State Key Laboratory of Green Biomanufacturing, Beijing University of Chemical Technology, Beijing 100029, China
* Correspondence: zhhl@buct.edu.cn

How To Cite: Jiang, Y.; Zhang, J.; Zhang, H.; et al. Methanol from Catalytic Conversion of Biogas-Based Syngas (CO, H_2). *Science for Energy and Environment* **2026**, *3*(1), 6. https://doi.org/10.53941/see.2026.100006

Received: 27 April 2026
Revised: 18 May 2026
Accepted: 18 May 2026
Published: 2 June 2026

Abstract: Hydrogen (H_2) will foster the decarbonization roadmap. H_2 faces challenges that hamper its application, storage and transport being the major issues needing reliable and affordable solutions. Its transformation into H_2-based green methanol offers a potential alternative. The present research applied a multi-step inter-cooled fixed-bed reactor using a $Cu/ZnO/Al_2O_3$ catalyst and fed with biogas-derived syngas of different CO/H_2 concentration ratios. The reaction is mainly carried out at 503 K and 5 MPa. Conversions and yields were measured after each of the 4 steps and revealed a total conversion of 97.8%. The catalyst was fully characterized and showed a nano-size structural cell with ultrafine crystallinity. Aspen simulation predictions using the Graaf et al. kinetic expressions accurately fitted the experimental results. The methanol purity exceeded 99.5%. The concept can be readily scaled up by using 3 successive catalytic beds with intercooling. Pilot-plant experiments will be further used to enhance the Technology Readiness Level.

Keywords: syngas (CO, H_2); methanol; catalyst; multi-step; fixed-bed; process result

1. Introduction

1.1. Background and Objectives

The transition toward a low-carbon future has intensified the need for sustainable routes to produce clean fuels [1–3] and value-added chemicals [4,5]. Among these, methanol has emerged as a versatile platform molecule as a hydrogen carrier, as a fuel, and as an intermediate for chemical industries. Conventionally, methanol is produced from fossil derived syngas. Biogas, generated from anaerobic digestion provides a promising alternative carbon source because it is abundant, renewable, and worldwide already produced at large scale [6]. Raw biogas consisting of mostly of CH_4 and CO_2 cannot be directly applied in methanol synthesis and must first be reformed into a syngas mixture with appropriate H_2/CO ratios. To accomplish this transformation, the dry reforming of methane (DRM) has attracted a particular interest owing to its simultaneous consumption of CH_4 and CO_2, thereby contributing to greenhouse gas mitigation [7,8]. Furthermore, the emergence of renewable hydrogen and carbon-capture technologies opens up opportunities to synthetically tailored biogas compositions and optimizes its conversion into syngas [9–11]. This research contextualizes the transition from biogas to syngas and its relevance for sustainable methanol production.

Although some literature data are available, there remains a lack of fundamentals of the multi-step intercooled reactor concept, of different operating pressures and GHSV-values. Therefore, our research effort has several fundamental and practical objectives:

- manufacture and characterize the $Cu/ZnO/Al_2O_3$ catalyst
- prepare the catalyst to a suitable size range for fixed-bed operation
- assess the optimum reaction pressure for a characteristic syngas
- determine the conversion and yields in a multi-pass catalyst bed (with intercooling)
- demonstrate the high yield and purity of the methanol produced
- assess the reactor stability for ~100 h of operation
- compare experimental and model-simulated results
- present a tentative scale-up system and recommend future research

1.2. From Biogas (CO_2, CH_4) to Syngas (CO, H_2)

1.2.1. Review of Biogas Production

Anaerobic digestion (AD) has been the subject of many research projects and publications, and is already applied on a large-scale to anaerobically convert organic material (biomass) into a solid bio-residue, biogas; and a nutrient-rich liquid digestate. Large-scale AD is used to treat various biodegradable waste (e.g., wastewater treatment sludge or agro-industrial residues such as manure) to recycle the useful nutrients and create the biogas. Different types of microorganisms play distinct roles in the four occurring stages of the process (hydrolysis, acidogenesis, acetogenesis and methanogenesis) [12].

To enhance biogas production and increase the CH_4/CO_2 ratio, different pretreatment methods have been implemented, as reviewed by Deng et al. [13] These methods increase the AD-hydrolysis kinetics, where ultrasonication, low-temperature (<383 K) pretreatments, and a two-stage AD system are the most cost-effective options for the industries. These pretreatment strategies can increase methane production by approximately 15–30%, depending on the feedstock and operating conditions. Such an increase in the CH_4/CO_2 ratio directly affects the downstream syngas conditioning and may require additional CO_2 adjustment to achieve the desired equimolar CO_2/CH_4 DRM feed composition and syngas stoichiometry for methanol synthesis. Non-AD CO_2, e.g., from CCSU, can be employed.

Although a higher CH_4 content in the anaerobic digestion gas is very appropriate for Combined Heat and Power (CHP) applications due to the higher calorific value of the biogas, the application in DRM needs additional measures to reach an equimolar composition as required by the DRM stoichiometry. These measures were already examined for common biogas (60/40 CH_4/CO_2) with a proposed integration of CCUS and a separate CH_4 catalytic decomposition into H_2 and value-added carbon nanotubes [3] whereafter the captured CO_2 was added to its lean main biogas stream.to achieve equal molarity with CH_4. With higher CH_4 to CO_2 ratios, this auxiliary step will need to be reinforced in the case of DRM applications, although a separate Reverse Water-Gas Shift (RWGS) step [$CO_2 + H_2 \rightarrow CO + H_2O$] will also help to reduce the CH_4-derived H_2 by increasing the required CO concentration for the methanol synthesis, where a molar ratio of 1 mol CO and 2 moles of H_2 (solely produced from CH_4 in DRM) can more easily be obtained.

The final step of methanogenesis will convert acetic acid into CH_4 and CO_2, which is called "biogas" and constitute over 90 vol% with methane (CH_4; ~60 vol%) and carbon dioxide (CO_2; ~35 vol%) as the major biogas components; but its composition differs with the source of the organic feedstock [14]. Table 1 summarizes the biogas composition with different organic streams feedstock.

Table 1. Biogas yields for various organic waste streams; adapted from [15].

	Concentrations				
	Vol %				**mg/m³**
	CH_4	**CO_2**	**N_2**	**O_2**	**H_2S**
Sewage sludge	65 ± 5	26 ± 7	<1	<0.5	500 ± 400
Domestic waste	55 ± 5	36 ± 2	<1	<1	2500 ± 1500
Manure	65 ± 5	26 ± 7	0–5	<0.5	6500 ± 3500

According to the IEA [16], biogas is now mainly used in Combined Heat and Power applications; although its use as a vehicle fuel is also envisaged. The worldwide number of AD plants exceeds 40,000 for Europe, USA, Australia, Asia and Brazil [16,17]. China has even higher number of AD plants as surveyed by Xu et al. [18]. These 110,000 plants deal with wastewater sludge or household waste (78.9%), agricultural residue (19.2%), and industrial residue (1.9%). The total annual biogas production exceeds 12.5×10^{12} m^3 of biogas [18].

Biogas compositions can also be "synthetically" composed by using CO_2 from Carbon Capture and Storage (CCS) plants and CH_4 (biogenic, or fossil fuel–based). Although possibly using a fossil source of CH_4, the C-balance after transformation to syngas is favorable.

1.2.2. Dry Reforming of Methane: From Biogas to Syngas

Methane Reforming

The current Steam Methane Reforming (SMR) uses C_{2+}-lean natural gas as the feedstock. It is a mature industrial process: high-temperature steam (973 K to 1273 K; 13 bar to 20 bar) reacts with CH_4 to produce H_2 and CO in the presence of a catalyst (Nickel-based). This gas mixture is also called syngas and has a high syngas ratio (H_2/CO = 3). The endothermic SMR is given in Reaction (1). A small amount of CO_2 and more H_2 are produced by the endothermic water-gas shift reaction of Reaction (2) [19,20]. SMR product gas is cleaned using the pressure swing adsorption (PSA) to remove CO_2 and other impurities, leaving a pure syngas stream [19]. The PSA purge gas can fire the steam boiler to drive endothermic reactions [20].

$$\begin{gathered} CH_4 + H_2O \rightarrow CO + 3H_2 \\ \Delta H^0_{298K} = 206\ \text{kJ/mol} \end{gathered} \tag{1}$$

$$\begin{gathered} CO + H_2O \rightarrow CO_2 + H_2 \\ \Delta H^0_{298K} = -41.2\ \text{kJ/mol} \end{gathered} \tag{2}$$

As alternative to SMR, is the Dry Reforming of Methane (DRM) process. Instead of using steam to convert methane, CO_2 is used, which is also the reason why it is called "dry". The endothermic and catalytic reaction is shown in Reaction (3) where a syngas is produced with a molar syngas ratio of 1 [21]. Whereas the produced biogas from an anaerobic digestion process often has a CH_4/CO_2 ratio of 60/40, the DRM stoichiometry for dry methane reforming ideally requires a 50/50 ratio, thus needing special attention when using biogas as a methane source.

$$\begin{gathered} CH_4 + CO_2 \rightarrow 2CO + 2H_2 \\ \Delta H^0_{298K} = 247\ \text{kJ/mol} \end{gathered} \tag{3}$$

In comparison with SRM, DRM has the benefits with respect to energy efficiency as no steam must be produced for the feed gas and by using CO_2, emissions of the greenhouse gases are reduced [22]. Despite having environmental benefits, DRM suffers from catalyst deactivation due to coke deposits as induced by the high-temperature methane decomposition, shown in Reaction (4). The second cause is the Boudouard Reaction (5), which occurs at lower temperatures. Finally, simultaneous Reaction (6) takes place by reducing the syngas ratio to below the theoretical unity [20].

$$\begin{gathered} CH_4 \rightarrow C + 2H_2 \\ \Delta H^0_{298K} = 75.0\ \text{kJ/mol} \end{gathered} \tag{4}$$

$$\begin{gathered} 2CO \rightarrow C + CO_2 \\ \Delta H^0_{298K} = -172.0\ \text{kJ/mol} \end{gathered} \tag{5}$$

$$\begin{gathered} CO_2 + H_2 \rightarrow CO + H_2O \\ \Delta H^0_{298K} = 41.2\ \text{kJ/mol} \end{gathered} \tag{6}$$

In the Partial Oxidation of Methane (POM), CH_4 and other natural gas hydrocarbons react with a limited amount of O_2 resulting in the formation of CO and H_2, with a syngas ratio of 2 since the limiting O_2 use is insufficient for complete oxidation with H_2O and CO_2 as the possible reaction products. Reaction (7) shows the reaction. Besides CO and H_2 as reaction products, a small amount of CO_2 is also formed according to water-gas shift reaction of the Reaction (2) [23].

$$\begin{gathered} CH_4 + 0.5\ O_2 \rightarrow CO + 2H_2 \\ \Delta H^0_{298K} = -23.0\ \text{kJ/mol} \end{gathered} \tag{7}$$

In comparison with other technologies, POM shows some advantages such as short required residence times, high reaction rates, no need for the catalyst, less sensitivity to fuel variations and it requires a smaller reactor than SRM. The downside of the technique is the need for pure oxygen as a reagent, which makes POM very expensive. Costs can be reduced by the recovery of a large amount of downstream heat.

Dry Reforming of Methane (DRM)

Various metal and carbonaceous catalysts have been investigated for reducing the temperatures applied in DRM and catalytic CH_4 decomposition (CDM). Both noble and non-noble metal-based catalysts are applied for the DRM process. Noble metals (Ru, Rh, Ir, Pt and Pd) offer an excellent coking resistance and activity specifically at higher temperatures [21]. Despite their benefits, noble metals are scarce and very expensive, hence hampering their application on an industrial scale. Non-noble metals like Ni, Co and Fe are the suitable alternatives for their lower cost, availability and their high activity. Coking remains a problem, but can be resolved using the support materials with alkaline characteristics such as MgO or CaO. The addition of minor amounts of noble metals creates a bimetallic synergistic catalyst [24]. The selection of active species carrier is of paramount importance since it needs to resist sintering and suppress carbon deposition [21]. Table 2 summarizes some DRM experiments, suggesting that Ni-based catalysts with different support materials have most widely been investigated and provide the highest conversions together with CeO_2.

Table 2. Literature results of dry methane reforming using different catalysts.

Catalyst	Metal (%)	Support	T (K)	Conversion		Reactor	Ref.
				CH_4	CO_2		
Ni	10	Al_2O_3	1073	94	93	Fluidized bed	[25]
Co	20	Al_2O_3	973	66	77	Fluidized bed	[26]
Ni	10	MgO	973	49	54	Fixed-bed	[27]
Ni	10	CeO_2	823	11.7	29.7	Fixed-bed	[28]
Ni	4.5	SiO_2	1023	47	60	Fixed/Fluidized-bed	[29]
Ni-Mo	5–25	SiO_2	1073	84	96	Fixed-bed	[30]
Ni-Ce	10–5	SiO_2	1073	81.4	87.5	Fixed-bed	[31]
Ni	12	Fleece	973	59.9	30.4	Fleece Reactor	[5]
CeO_2	10	Fleece	1073–1173	97.4	88.4	Fleece Reactor	Our work

The Future of E-Methanol

The syngas could be split into H_2 and CO, but both gases have advantages and disadvantages. For CO, the major drawback is its toxicity and moderate calorific value only. Upon combustion, it produces CO_2 and hence no longer meeting the C-neutrality target. Produced H_2, on the other hand [2,4,13,32], has merits of a high energy density, clean combustion, and potential direct fuel or feedstock application in important production processes such as fertilizers, steel, cement among others. However, a critical H_2 challenge remains its storage and transportation, with diffusion through most metals and polymers, steel embrittlement and pipe damage as the major concerns. This limits pipeline transportation, especially when at higher pressures.

Novel, efficient, and reliable affordable solutions are needed to foster the potential. The conversion into easily storable liquid E-methanol offers a solution, which is the target of the present research. This e-methanol priority was also proposed by Liebreich [33] who ranked economically interesting application processes according to their economic potential. The immediate market potential for e-methanol is estimated at 90 Mton/year [34]. E-methanol would moreover reduce the environmental and energy burdens of the current fossil-fuel-based methanol; with emissions between 5 tons and 8 tons of CO_2/ton CH_3OH produced, requiring an energy input of 8–10 MWh/ton CH_3OH [34].

Several methanol synthesis processes have been proposed in the literature, including multi-stage fixed-bed reactors with intercooling [3], membrane-assisted methanol synthesis [35], CO_2 hydrogenation routes using renewable H_2 [36,37], and intensified e-methanol production systems integrated with carbon capture technologies [38]. These processes aim to improve syngas conversion, methanol selectivity, thermal management, and overall process sustainability, thereby supporting the transition toward low-carbon fuel and chemical production. The multi-stage fixed-bed reactor has been favored for its flexibility and easy scale-up. A recent publication by our team [3] reviewed the fixed-bed methanol synthesis developments toward the reactor configurations and their temperature profile. It selected a multi-bed configuration for a syngas-to-methanol reactor, as illustrated in Figure 1. A reactor of CH_3OH synthesis in single, double, triple, or quadruple stage was applied in that research. It also reviewed the kinetic models and their use in an Aspen simulation package. The results of the simulation compared to our experimental results are provided in Section 4.1.

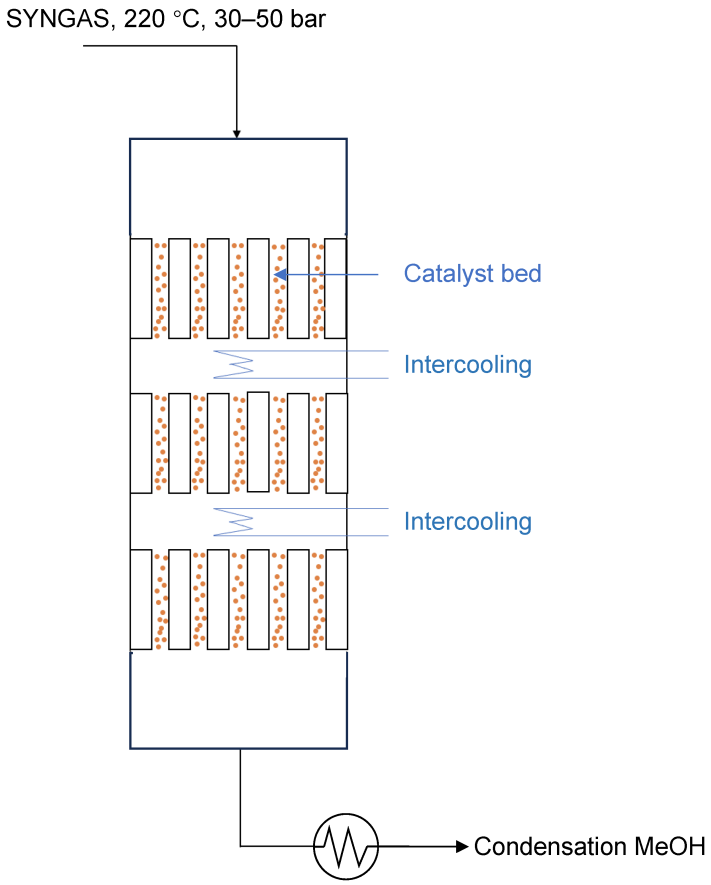

Figure 1. Multi-tube triple-stage fixed-bed catalytic reactor with required inter-cooling from 523 K to 493 K due to reaction exothermicity.

Since methanol synthesis is a strongly exothermic reaction, with a reaction enthalpy of −90.55 kJ/mol, temperature control inside the catalyst bed is of major importance to avoid catalyst overheating and equilibrium limitations. Therefore, an intercooled multi-stage fixed-bed reactor concept was selected in the present work. Between successive catalytic stages, the reaction gas is cooled by heat exchange with water, where the evaporation of water absorbs the released reaction heat. This interstage cooling maintains near-isothermal operating conditions, improves methanol equilibrium conversion, and enhances catalyst stability.

Previous lab-scale research was investigated and illustrated catalytic combinations that were assessed. All results were obtained for a high GHSV (despite being operated at low STP conditions). Pressures vary from 3 MPa to 7.5 MPa, and temperatures of the operation are between 493 K and 543 K. The production of methanol, expressed as STY, varies considerably with the highest values obtained for $Cu/ZnO/Al_2O_3$ catalysts at 5 MPa and at ~503 K.

Successive steps are required to clean the discharges from the methanol reactor. A flash unit separates methanol from the unreacted syngas, water, methane, CO_2 and inerts. Methanol and water, called crude methanol, are condensed at 313 K. The flashed top-stream gases are mostly recycled to the feedstock reactor to enhance the conversion yield. To avoid the accumulation of inerts in the recycle stream, a small fraction (~2%) is purged. Subsequently, crude methanol will be distilled to achieve the desired purity of methanol to between 99.5% and 99.85% (for AA grade methanol 99.85% is required).

2. Materials and Methods

2.1. Reactants

All the reagents used in this work were of analytical grade, supplied by Macklin Chemical Reagent Beijing Co., Ltd. (Beijing, China); and used without further treatment.

2.2. Catalyst Preparation

A 1 mol/L solution of $Cu(NO_3)_2{\cdot}3H_2O$, $Zn(NO_3)_2{\cdot}6H_2O$ and $Al(NO_3)_3{\cdot}9H_2O$ was prepared by dissolving these nitrates in de-ionized water. A solution with 1.0 mol/L CO_3^{2-} was prepared by dissolving sodium

carbonate in deionized water, and used as a precipitant. In the co-precipitation process, at 343 K, aqueous solutions of $Al(NO_3)_3$ and Na_2CO_3 were simultaneously and progressively added into the flask under vigorous stirring, while maintaining the pH between 7.9 and 8.3 by adjusting the feed rate of the carbonate solution. The obtained suspension was aged for 30 min. Subsequently, aqueous solutions of $Cu(NO_3)_2$ and $Zn(NO_3)_2$ and Na_2CO_3 were simultaneously added into the flask following the same co-precipitation procedure. After the addition, the suspension was aged at 343 K for 2 h.

The obtained precipitate was washed with de-ionized water, filtered until a neutral filtrate was obtained, followed by drying at 383 K for 12 h to obtain the catalyst precursor. The precursor was then calcined (623 K, 4 h at 2 K min^{-1}). The catalyst was finally H_2-reduced according following the procedure of Willinger et al. [39] to selectively reduce only CuO. The reduced material was pelletized, milled, and sieved between 420 μm and 850 μm. These particles were then used as the catalyst in the methanol (CH_3OH) reactor.

2.3. Catalyst Properties

The microstructure and crystallinity of the catalysts were determined by X-ray diffraction (XRD) using a Bruker D8 ADVANCE diffractometer equipped with an AUTOCHANGER sample feeder. The crystallite size of the metallic Cu in the reduced catalyst was determined from the Scherrer equation at the full width at half maximum (FWHM) of Cu(111) peak at 2θ = 43.23°. Textural properties (BET, pore volume, average pore diameter) were measured by N_2 adsorption–desorption measurements (Micromeritics Tristar 3000 analyzer). Pore volume and average pore size were obtained using the Barrett–Joyner–Halenda (BJH) model for the desorption. The sample morphology was examined by a Nova NanoSEM 450 scanning electron microscope (FEI, USA). The elemental distribution and compositions were analyzed by Oxford X-Max 50 energy-dispersive X-ray spectroscopy (EDS) detector. Prior to SEM observation, the samples were sputter-coated with Au to improve their conductivity. The catalyst microstructure was examined using TEM (JEOL JEM-ARM200F). The microscope was equipped with an Oxford X-MaxN 100 TLE EDS detector using Mn Kα as the calibration source.

2.4. Experimental Detailst

CH_3OH Synthesis Reaction in a Fixed Bed Pellet Reactor

The fixed bed pellet reactor was built for this purpose based on our design by Boyue Filtration Equipment Manufacturing Co. Ltd. (Xinxiang, China). It is illustrated in Figure 2.

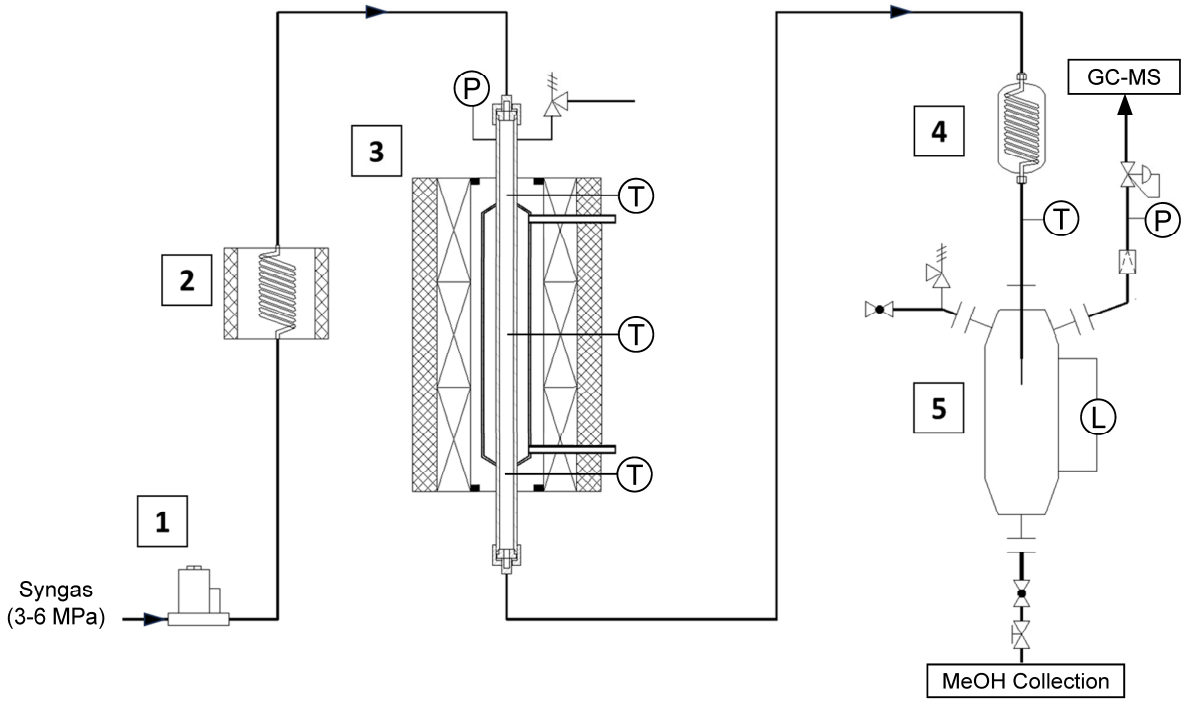

Figure 2. Experimental single fixed-bed reactor. (1) flowmeter; (2) pre-heater; (3) reactor; (4) glycol-water cooler (268.15 K); (5) high pressure condenser/segregator.

The overall experimental setup is illustrated in Figure 3.

The catalytic performance was carried out in the tubular fixed-bed reactor (inner diameter: 10 mm). One to five grams of the catalyst was compressed at 10 MPa into pellets, crushed, and sieved to 420–850 μm to minimize the intraparticle diffusion limitations. The catalyst was then homogeneously diluted to 10 g with quartz sand of the same mesh size and loaded into the isothermal zone at the center of the reactor. Additional quartz sand (420–850 μm) was packed upstream and downstream to keep the catalyst bed in place. Prior to the reaction, the catalyst was again reduced at 503 K under 10% H_2/N_2 flow for 3 h whereafter catalytic tests were performed under the desired reaction conditions. Measurement of the effluent gas products was carried out using an online gas chromatograph (Beifen-Ruili Analytical Instrument Co., Ltd. Beijing, China). The system was equipped with two thermal conductivity detectors (TCDs) and Hayesep A, GDX-104, and molecular sieve 5A columns for gas separation and analysis. The concentrations of H_2, CO, CO_2, CH_4, N_2 were continuously monitored throughout the reaction process. The condensed liquid methanol products collected in the cold trap were further analyzed using an offline Shimadzu GC-2014 gas chromatograph equipped with a flame ionization detector (FID) and a SH-5 capillary column.

Figure 3. Photograph of the fixed-bed pellet reactor.

3. Results and Discussion

3.1. Catalyst Properties

The $Cu/ZnO/Al_2O_3$ catalyst (molar ratio of 6:3:1) was synthesized as described in Section 2.2.

The catalyst properties are reported in detail by Jiang et al. [40]. Relevant data are summarized below.

Selective reduction reduces CuO to Cu. The Cu crystallite size is 6.99 nm and ZnO is 2.94 nm, indicating that the catalyst has extra fine crystallites, beneficial for gas-catalytic reactions. As shown in the Figure 4, SEM images of the calcined catalyst particles show the existence of fiber-like, plate-like and irregular aggregated morphologies. After reduction, a clearer porous texture is observed, indicating beneficial enhanced surface accessibility and gas adsorption capability. After the reaction, the catalyst particles show numerous small granular structures, however without changing BET and pore characteristics. Figure 5 and Table 3 has been incorporated to more clearly emphasize that the catalyst did not exhibit significant degradation during the investigated reaction period since pore size and pore volumes do not change between the virgin and spent catalysts. The fact that no loss of yield, conversion and selectivity was

recorded for several repeat and successive long-duration experiments with the same catalyst, supports the presumed stability of the catalyst and the absence of e.g., catalyst coking.

The low-magnification TEM image (Figure 6) reveals that the catalyst is composed of agglomerated nanoparticles with irregular shapes and a broad size distribution, which is characteristic of materials prepared by co-precipitation. The HRTEM image reveals well-resolved lattice fringes resulting from the presence of highly ordered crystalline domains.

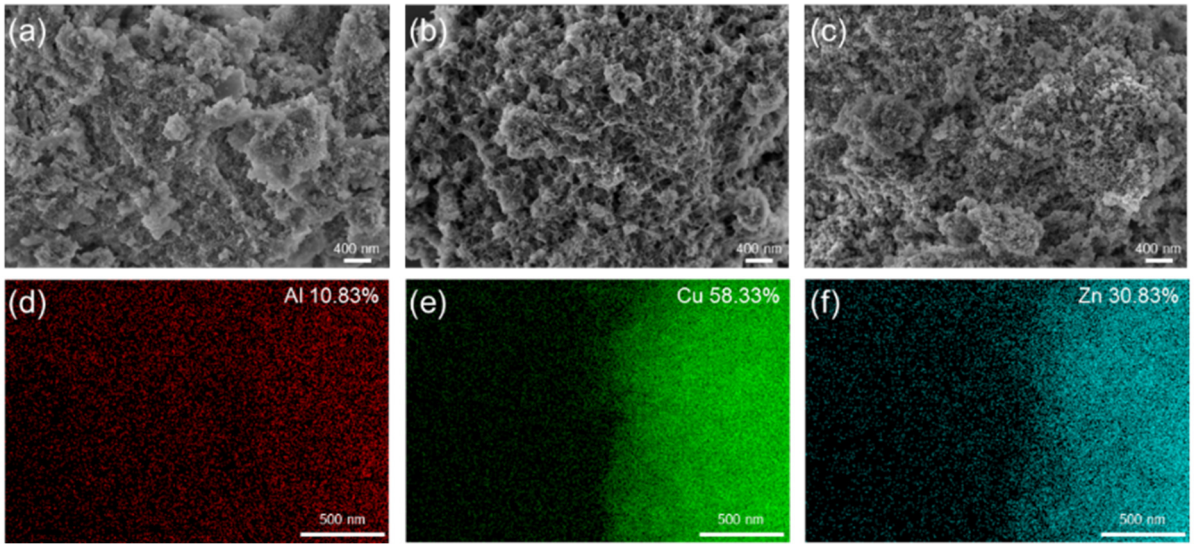

Figure 4. SEM images of (**a**) calcined, (**b**) reduced and (**c**) reacted catalyst samples (scale bar: 400 nm) and (**d**–**f**) EDS images of reduced catalyst samples (scale bar: 500 nm).

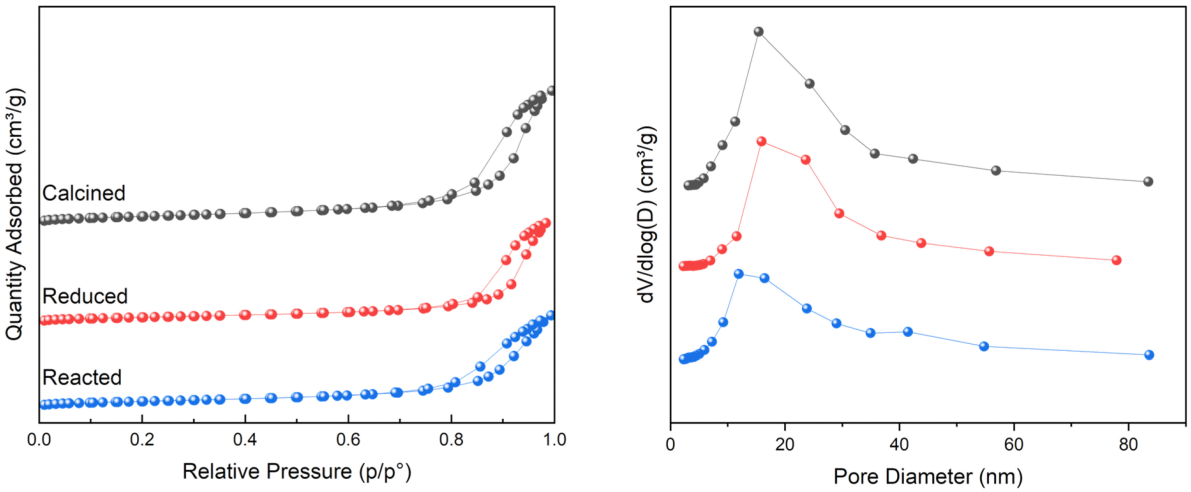

Figure 5. Absorption/desorption isotherms (**a**) and pore size distributions (**b**) for the catalyst at calcined (black), reduced (Red) and reacted (Blue) $Cu/ZnO/Al_2O_3$ conditions.

Table 3. Textures of calcined, reduced and reacted catalysts.

Sample	BET ($m^2 \cdot g^{-1}$)	Pore Volume ($cm^3 \cdot g^{-1}$)	Pore Diameter (nm)
Calcined	70.7	0.4	16.3
Reduced	49.7	0.3	17.9
Reacted	57.1	0.3	15.1

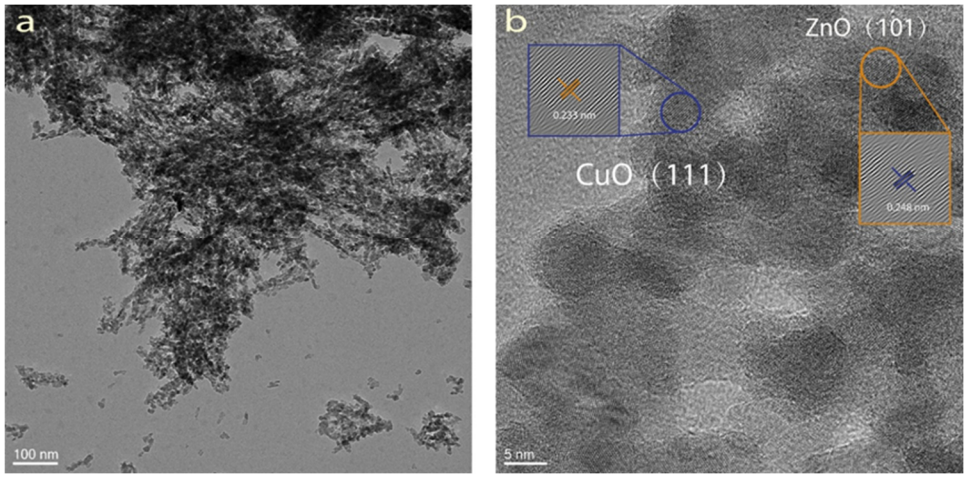

Figure 6. (**a**) TEM image of the Cu/ZnO/Al_2O_3 catalyst; (**b**) its HRTEM image.

3.2. Methanol Production Yield

Triplicate experiments have deviations with the average values mostly below 0.5%. Error bars can therefore not visually be presented in the figures, except for a single data point. In the methanol production, both CO and CO_2 hydrogenation proceed simultaneously, according to the following reactions:

$$CO + 2\,H_2 \rightleftharpoons CH_3OH \quad \Delta H_{298} = -90.55\ \text{kJ/mol} \tag{8}$$

$$CO_2 + 3\,H_2 \rightleftharpoons CH_3OH + H_2O \quad \Delta H_{298} = -90.55\ \text{kJ/mol} \tag{9}$$

$$CO_2 + H_2 \rightleftharpoons CO + H_2O \quad \Delta H_{298} = 41.2\ \text{kJ/mol} \tag{10}$$

3.2.1. Operating Pressure

Higher pressures are beneficial but cost more compression energy. Operating at pressures above 5 MPa only slightly improves the H_2 conversion, as shown in Figure 7. The results are consistent with the Le Chatelier principle, since higher pressures favour conversions due to the overall net decrease in product gas moles.

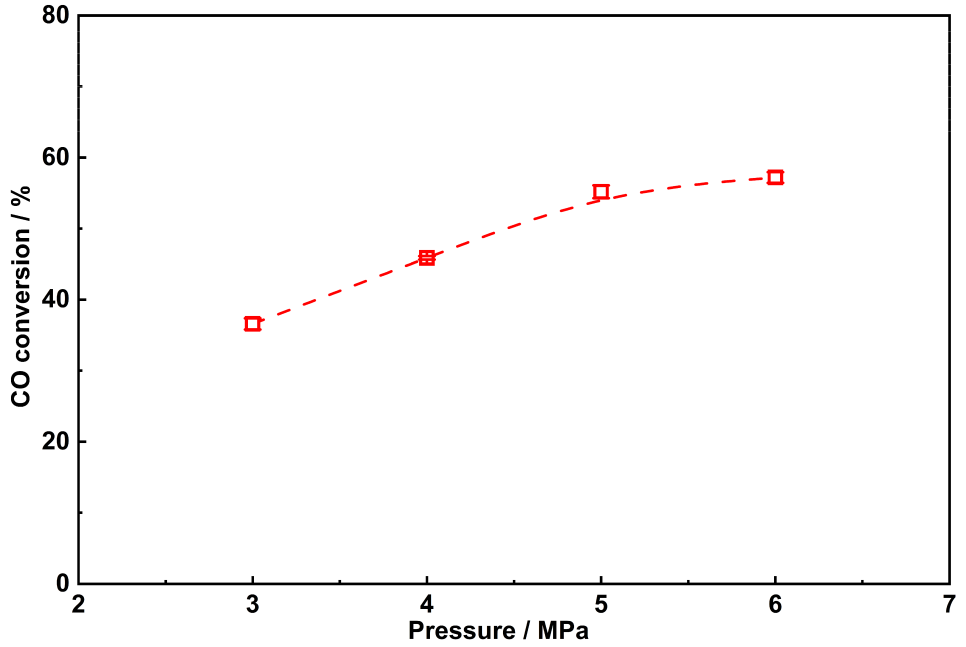

Figure 7. CO conversion at 503 K for different operating pressures in the first step of the multi-step reaction system.

3.2.2. Operating GHSV

The effect of GHSV on the CO conversion in $Cu/ZnO/Al_2O_3$ system was evaluated at a constant 503 K and 5 MPa. The results are presented in Figure 8.

Lower GHSV favors higher CO conversion, due to longer residence time and closer approach to equilibrium, as expected from the kinetics and thermodynamics of catalytic methanol synthesis over $Cu/ZnO/Al_2O_3$ catalysts. The influence of GHSV on the reaction kinetics is discussed in Section 3.3.

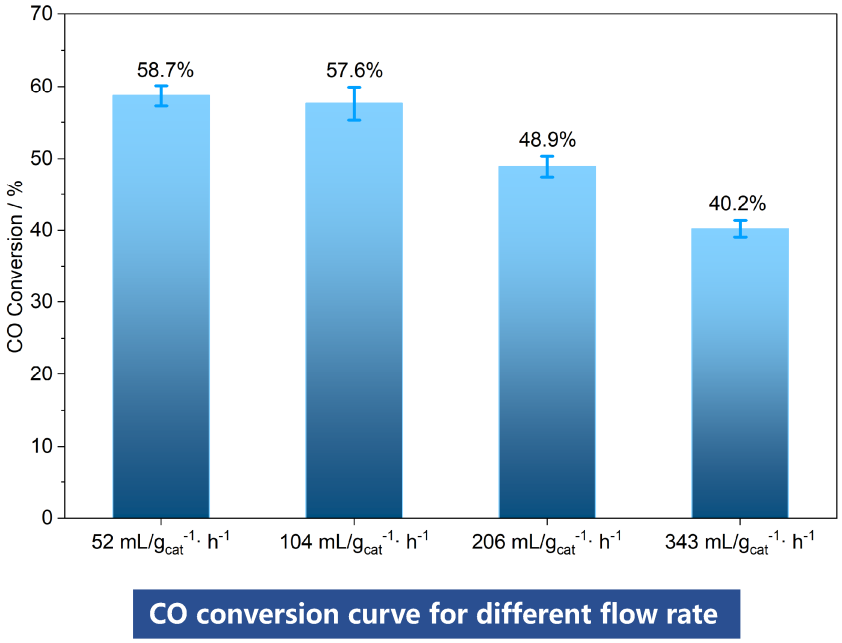

Figure 8. CO conversion with different flow rate at 5 MPa and 503 K in a single step mode.

3.2.3. Effect of Single, Double, Triple, Quadruple Successive Reactions

To simulate the progression of loop reactions in industrial methanol synthesis, the outlet gas compositions from different operating stages were introduced into the same reactor under identical temperature and pressure. The detailed feed compositions for each stage are given in Figure 9 that shows gas composition progressively changed along the four simulated recycle stages. With the evolution of reaction atmosphere, the overall CO conversion continuously increased and eventually reached 97% in Stage IV. At this stage, the catalyst also exhibited excellent selectivity toward methanol. The main by-product was methane, but only in trace amounts. Unlike conventional single-pass fixed-bed methanol reactors commonly reported in literature (as illustrated in Table 2), the present research applies a multi-stage intercooled fixed-bed reactor configuration specifically designed for biogas-derived syngas conversion. The reactor concept combines successive catalytic reaction stages with intermediate cooling, thereby reducing local overheating caused by the exothermic methanol synthesis reaction and maintaining more favorable near-isothermal operating conditions. In addition, the staged configuration progressively increases the overall CO conversion while preserving high methanol selectivity and catalyst stability. This reactor concept therefore differs from conventional reactor systems by integrating reaction staging, intercooling, and recycle-stage simulation within a compact laboratory-scale fixed-bed setup.

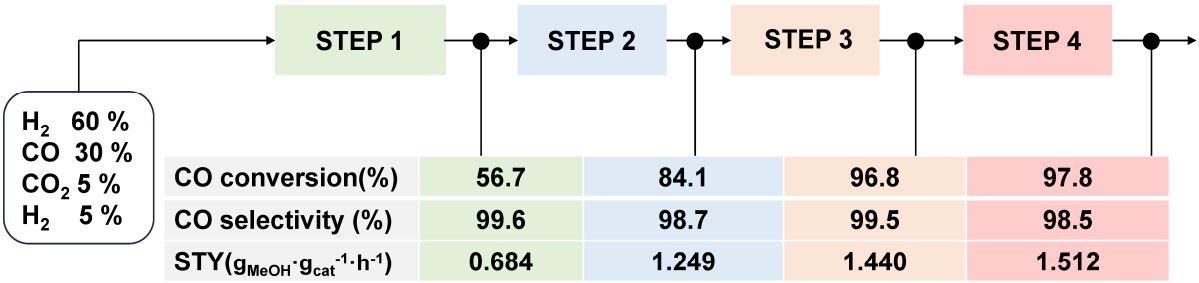

Figure 9. Performance of methanol synthesis at the different stages (P = 5 MPa, T = 503 K).

The experimental gas-phase analysis showed a nearly constant CO_2 concentration, demonstrating that the reverse water–gas shift reaction is of minor impact at temperatures below 573 K. Therefore, CO is considered the dominant carbon source for methanol formation. Accordingly, the CO conversion was selected as the most appropriate indicator of catalytic activity, and accepts as RDS (Rate-determining step). Figure 10 presents the corresponding results.

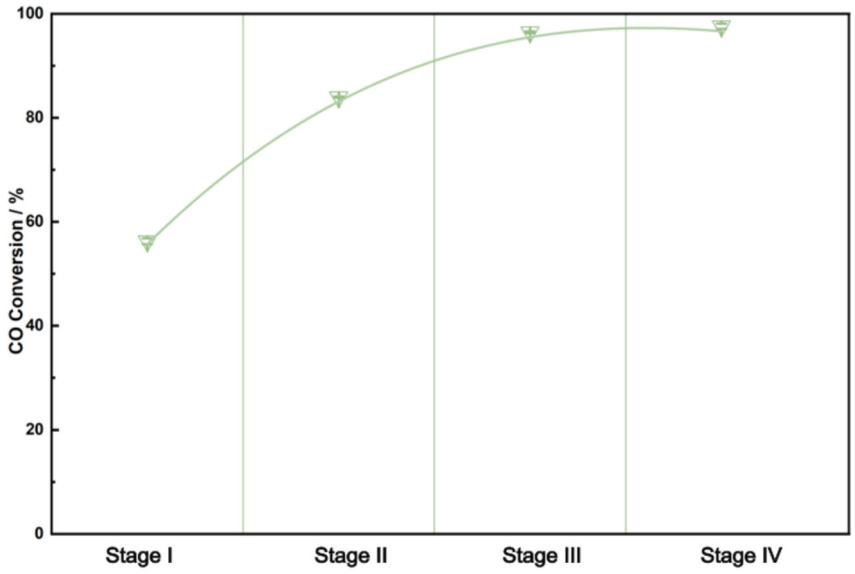

Figure 10. Total CO conversion at equilibrium at different stages.

The methanol purity was defined by GC and revealed a value more than 99.5%. Trace of H_2O were detected, probably formed by the RWGS.

3.3. Reaction Kinetics

The kinetic expressions for the synthesis of CH_3OH vary widely, with adsorption, desorption and chemical reaction rate as main overall kinetic resistances. Adsorption and desorption processes are generally considered to be close to quasi-equilibrium under the investigated operating conditions, while the surface reaction is more likely to control the overall reaction rate, as commonly discussed in heterogeneous catalytic kinetic studies such as those reported by Everaert et al. [41], where the complex Langmuir-Hinshelwood-Hougen-Watson (LHHW) approach where chemisorption, desorption, as well as the surface reactions are all included [42], can be reduced to a kinetic approach where the CO conversion is the rate-determining step (RDS). This was recently also validated for the DRM reactions [5]. The overall reaction mechanism indeed involves steps of adsorption, surface reaction, and desorption. Desorption is very fast (endothermic process) at the operating temperature, and is therefore not a limiting resistance. Provided an appropriate catalyst is selected, adsorption is very fast since CO readily adsorbs onto active sites of both the metal or support to form surface oxygen complexes; which promptly react with the H_2 species to form methanol. Reaction mechanism steps of CO-adsorbate dissociation and its reaction with H_2 can hence be considered as essential parts of the surface reaction [43–46], thus limiting a complex LHHW model to its Eley-Rideal form, resulting in a power law kinetic expression where both concentrations of H_2 and CO are dominant, as proposed in the kinetic model approach of the paper. The competing Boudouard reaction would lead to coking, not experimentally observed and hence considered of negligible impact. The kinetic expression can hence be expressed in terms of the reaction rate at RDS. For sake of completeness, the LHHW approach, as applied by Graaf et al. [47] was examined by comparing the experimental and predicted RDS kinetics, and by using the complete Graaf et al. approach in an ASPEN simulation. Considering CO as being the RDS, a simplified approach is possible, based upon the reaction stoichiometry and the 1/2 CO/H_2 feed composition.

Since in the present research, mostly syngas (90% CO + H_2) and 5% CO_2 were applied, the reaction kinetics are determined by the three parallel reactions (Section 3.2), although reaction 10 will preferentially proceed due to the higher CO concentration. It was moreover experimentally demonstrated that no water was formed.

The kinetics of 10 can thus be expressed as:

$$\frac{d(CH_3OH)}{dt} = k[CO][H_2]^2$$

and

$$\frac{d(CO)}{dt} = -k[CO][H_2]^2$$

Since the concentrations of CO and H_2 in the feedstock are fixed in a 1-to-2 molar ratio and since the conversion of H_2 and CO proceed stoichiometrically, the reaction can be expressed for equal molar concentrations as:

$$\frac{d(CO)}{dt} = -k[CO][2CO]^2 = -4k[CO]^3$$

with x as concentration of reactant (CO) transformed at time t.

$$\frac{dx}{dt} = -4k(a-x)^3 \quad \text{(with the initial concentration)}$$

Integrating from $t = 0$ to $t = t$ and from a to x, the equation becomes:

$$k = \frac{1}{2(t_2 - t_1)}\left[\frac{1}{(a-x_1)^2} - \frac{1}{(a-x_2)^2}\right]$$

To apply the equations into Arrhenius equation, results at different temperatures T and contact times are required with x respectively at t_2 and t_1. Such experiments were conducted with $Cu/ZnO/Al_2O_3$ catalyst at initial syngas concentrations of 30% CO and 60% H_2, hence justifying the kinetic simplification, due to the correct molar ratio of CO and H_2.

From the experimental results of CO-conversions at different times (corresponding to different GHSV-values), with 1 g catalyst at 5 MPa, the k-value for CO-methanol conversion was from the above equation as $k = 2.63 \times 10^{-7} \frac{kmol}{kg_{cat}} \cdot s \cdot Pa$. Using the activation energy, E_a, as determined by Graaf et al. [47], i.e., 11,695 J/mol, the complete expression for k becomes

$$k = 4.31 \times 10^{-6} \exp\left(\frac{-11{,}695}{RT}\right) \text{ kmol/kg}_{cat} \cdot \text{s} \cdot \text{Pa}$$

It should be noted that Graaf et al. equation proposes a pre-exponential factor of 4.064×10^{-6}, hence deviating only by 5.8% from our experimental value [47], which is certainly acceptable in view of the accuracy of the GC–MS measurements. With the determined E_a and A values, the conversion at different values of T, t and C_0 can be calculated.

4. Scale-Up

4.1. Aspen Simulation

In the Aspen Plus® V12.1 simulation, the well-known and robust Graaf et al. [47] kinetic model is used since the feed contains CO (without CO_2) thus limiting the rWGSR and pressure around 5 MPa are applied.

The Graaf et al. kinetics adopts the LHHW model, for thermodynamic properties, property methods PSRK and NRTL were used for high and low pressure units, respectively. The PSRK, or "Predictive Soave-Redlich-Kwong" method is used to calculate the phase equilibria of mixtures of chemical components where the established methods, e.g., UNIFAC fail [48–52]. The NRTL, or "Non-Random Two-liquid Model", as introduced by Renon and Prausnitz [53,54] correlates the activity coefficients of a compound with its liquid molar fraction.

For the amount and composition of the feed stream, DRM, syngas, was used. Methanol synthesis was simulated at 5 MPa and 498 K. A $Cu/ZnO/Al_2O_3$ catalyst with a bed voidage of 0.4 and a density of 1175 kg/m^3 was used. The reactor is a 3-stage multi-tubular reactor which is cooled by water.

The incomplete reaction in a single-pass catalytic synthesis is common to gas-catalytic processes. The recycle stream will be redirected to the feed side of the reactor. The 3.24% purge is considered as a waste stream, but can be used in heat generation. It should moreover be remembered that the Aspen Plus simulation limits the reaction section to three successive near-isothermal parts. A further extension to deeper catalyst beds or to extra sections will undoubtedly increase the H_2/CO conversion rates and further limit the recycle flows. A full and up-to-date review of the Aspen simulation was recently presented by our team [13]. Only essential facts are reported below.

The methanol production yield is ~98.6%, in close agreement with the experimental results as illustrated in Figure 11.

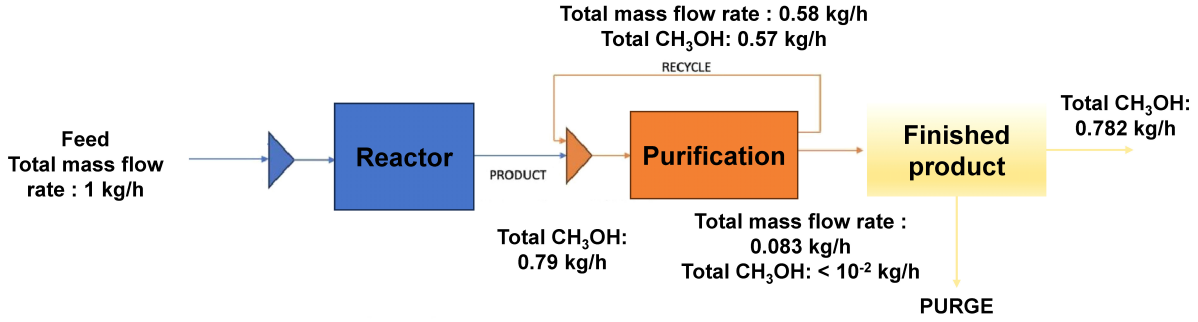

Figure 11. Aspen simulation results for a syngas mass flow rate feed rate of 1 kg/h.

4.2. Scale-Up Layout of the Reactor

For further tests, we have already purchased a 2-step reactor as shown in Figure 12. The feed gas needs to be pre-heated to 483–493 K, whereas the reactor will operate exothermally at 503 K. The intercooling circuit will generate pressurized water (3 bar at ~373 K).

4.3. Economic Concerns about the E-Methanol Synthesis

The economics of the process are mostly impacted by the costs of compressing the gaseous feedstock to 5 MPa. Heat requirements are low due to the relatively low reaction temperature and the exothermic nature of the reaction, with a possible and required heat recovery for e.g., the feedstock preheating. For the production of 1 kmol/h of methanol, 3 kmol/h of gaseous feedstock need to be compressed. With the molar weight of methanol and the molar volume of CO and H_2, each 32 kg/h of methanol requires the compression of 2.1 Nm^3/h of CO and H_2. A 3-stage compression with intercooling will be used. The compression energy is given by

$$P\,(\mathrm{kW}) = 0.0114\, P_d\, V_d\, [1 - P_0/P_d)^{0.286}]/\eta$$

with P_0 and P_d, in P_a, the inlet (0.1 MPa) and discharge pressure (5 MPa), respectively. V_d is the gas flow rate in m^3/s at discharge condition; and η is the power generating efficiency of the compressor (on average 85%). Applied to the 32 kg/h methanol case, V_d is ~0.00037 m^3/s. The power consumption, P, is ~16 kW. At 0.10 €/kW, the power costs are 1.6 € per 32 kg/hr of methanol (about 240 T/yr), or 0.05 €/kg. In comparison with the current market value of methanol (0.5–0.55 €/kg); the major compression cost of the reaction system represents less than 10%.

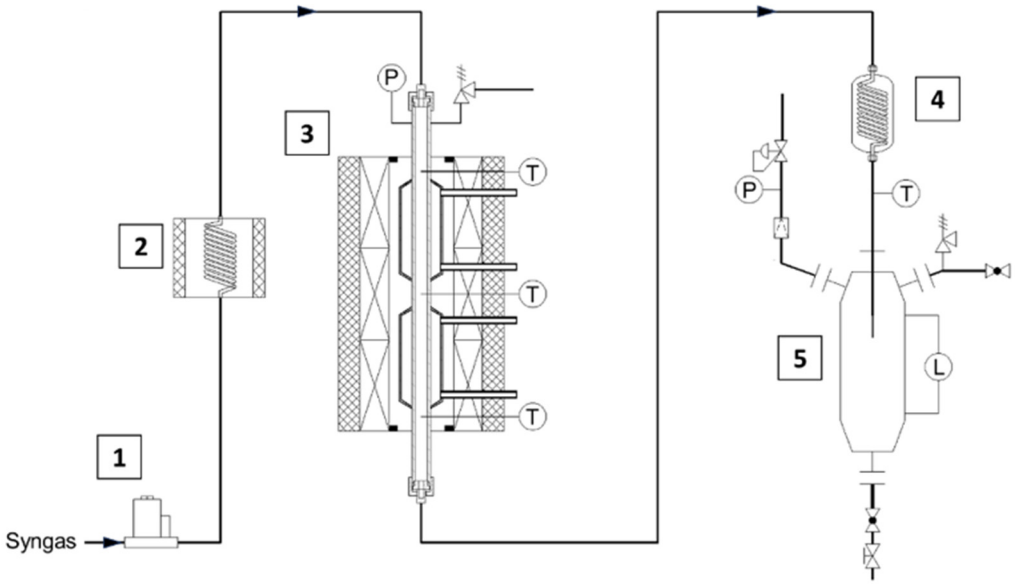

Figure 12. Experimental layout of the 2-step fixed-bed pellet reactor. (1) Flowmeter (2) Preheater (3) Reactor (4) Glycol/water Cooler (5) High pressure condenser.

5. Conclusions

It is generally accepted that production of methanol from syngas belongs to the required "green synthesis" methods. The reported research applied a 4-stage fixed-bed reactor fed with syngas of different CO/H_2 concentration ratios. Methanol synthesis was mainly carried out at 503 K and 5 MPa using a co-precipitated $Cu/ZnO/Al_2O_3$ catalyst. The catalyst was fully characterized and showed a nano-sized structural cell with ultrafine crystallinity of 6.99 nm for Cu and 2.94 nm for ZnO. The conversions and yields were measured after each of the 4 steps and revealed a total conversion of 56.7% after step 1, 84.1% after step 2, 96.8% after step 3, and 97.8% after a 4th step. Operating at 5 MPa exceeded results at lower pressures, and operating at 6 MPa only slightly improved the results. The CH_3OH yield was close to 98%, with a purity more than 99.5%. Aspen Plus® simulation and confirmed our results. Using deeper near-isothermal catalyst beds will undoubtedly increase the H_2/CO conversion rates. The research only proves the concept making full economic assessment premature. This will be included as a follow-up path further to pilot-scale research (TRL = 3 to 5). Overall, it can be confirmed that methanol synthesis from the syngas is a feasible and reliable operation.

Author Contributions

Y.J.: Investigation, Experiments; writing. J.Z.: Funding acquisition, Methodology, Writing and Editing. H.Z.: Methodology, Data treatment, Writing and Editing. J.B.: Conceptualization, Project Administration, Writing and Editing. All authors participated in the Final Review and Writing. All authors have read and agreed to the published version of the manuscript.

Funding

Authors express their gratitude for funding to the Beijing Advanced Innovation Center for Soft Matter Science and Engineering of Beijing University of Chemical Technology, and to the National Key R & D Program of China [grant number 2021YFC2103705].

Data Availability Statement

Additional data will be made available upon a request with the corresponding author.

Conflicts of Interest

The authors declare no conflict of interest.

Use of AI and AI-Assisted Technologies

No AI tools were utilized for this paper.

Abbreviations and Symbols

AD	Anaerobic Digestion
CCS	Carbon Capture and Storage
CDM	Catalytic decomposition of methane
POM	Partial Oxidation of Methane
SMR	Steam Methane Reforming
PSA	Pressure swing adsorption
DRM	Dry reforming of methane
RDS	Rate-determining step
LHHW	Langmuir-Hinshelwood-Hougen-Watson
PSRK	Predictive Soave-Redlich-Kwong
NRTL	Non-Random Two-liquid Model
GHSV	Gas hourly space velocity ($mL/g_{cat}·h$)
TRL	Technology Readiness Level
A	Arrhenius pre-exponential factor (1/s)
$[H_{2,in}]$, $[H_{2,out}]$	Molar initial or outgoing flowrate of H_2 (mol/h)
$[CO_{in}]$, $[CO_{out}]$	Molar feed or outflow of CO (mol/h)
Ea	Activation energy (J/mol)
kgcat	Catalyst weight (kg)
k	Reaction rate constant (1/s)
R	Universal gas constant (J/mol.K)
t	Contact time (s)

wt%	Weight percent (%)
FWHM	Full width at half maximum
STY	Space time yield (g_{MeOH}/g_{cat}·h)
STP	Standard temperature and pressure

References

1. Zhang, H.; Fang, Y.; Wang, M.; et al. Prospects and perspectives foster enhanced research on bio-aviation fuels. *J. Environ. Manag.* **2020**, *274*, 111214. https://doi.org/10.1016/j.jenvman.2020.111214.
2. Deng, Y.; Dewil, R.; Appels, L.; et al. Hydrogen-enriched natural gas in a decarbonization perspective. *Fuel* **2022**, *318*, 123680. https://doi.org/10.1016/j.fuel.2022.123680.
3. Zhang, H.; Kou, Y.; Yang, M.; et al. Producing "green" methanol from syngas, derived from anaerobic digestion biogas. *Front. Chem. Sci. Eng.* **2025**, *19*, 92. https://doi.org/10.1007/s11705-025-2549-y.
4. Deng, Y.; Baeyens, J.; Margot, V.E.; et al. Renewable electricity and "green" feedstock-based chemicals will foster industrial sustainability. *Innov. Energy* **2024**, *1*, 100016. https://doi.org/10.59717/j.xinn-energy.2024.100016.
5. Chu, F.; Jiang, Y.; Li, Z.; et al. Sustainable Biogas-to-Syngas Catalytic Dry Reforming of Methane (DRM) Using a Novel Fleece Reactor. *Sustainability* **2026**, *18*, 3151. https://doi.org/10.3390/su18063151.
6. Kiran, E.U.; Stamatelatou, K.; Antonopoulou, G.; et al. 10—Production of biogas via anaerobic digestion, In *Handbook of Biofuels Production*, 2nd ed.; Luque, R., Lin, C.S.K., Wilson, K., et al., Eds.; Woodhead Publishing: Cambridge, UK, 2016; pp. 259–301. https://doi.org/10.1016/B978-0-08-100455-5.00010-2.
7. Chao, C.; Deng, Y.; Dewil, R.; et al. Post-combustion carbon capture. *Renew. Sustain. Energy Rev.* **2021**, *138*, 110490. https://doi.org/10.1016/j.rser.2020.110490.
8. Guastaferro, M.; Marchetti, L.; Baglioni, F.; et al. Efficient syngas generation from heterogeneous waste for low-carbon methanol synthesis. *Fuel* **2026**, *420*, 138952. https://doi.org/10.1016/j.fuel.2026.138952.
9. Deng, Y.; Margot, V.E.; Liu, H.; et al. Techno-economic feasibility and kinetic optimization of dry reforming of methane. *J. Environ. Chem. Eng.* **2026**, *14*, 121021. https://doi.org/10.1016/j.jece.2025.121021.
10. Alamdari, A.; Azarhoosh, M.J.; Aghaeinejad-Meybodi, A. Thermodynamic assessment of tri-reforming of methane with optimization of operating conditions to achieve suitable syngas for methanol production. *Sci. Rep.* **2026**, *16*, 14257. https://doi.org/10.1038/s41598-026-44472-x.
11. Olazar, L.; Pawelczyk, E.; Gębicki, J.; et al. Evaluation of continuous pyrolysis and in-line catalytic dry reforming of commodity plastics for syngas production. *Fuel* **2026**, *426*, 139476. https://doi.org/10.1016/j.fuel.2026.139476.
12. Sudalyandi, K.; Jeyakumar, R. *Biofuel Production Using Anaerobic Digestion*, 1st ed.; Springer: Singapore, 2022. https://doi.org/10.1007/978-981-19-3743-9.
13. Deng, Y.; Li, S.; Liu, H.; et al. Recent Research in Solar-Driven Hydrogen Production. *Sustainability* **2024**, *16*, 2883. https://doi.org/10.3390/su16072883.
14. Ramli, S.; Baki, A.M.; Ayub, M.A.; et al. Renewable Energy from Biogas Generated by Sewage Sludge—Relationship between Sludge Volume and Power Generated. *Sci. Res. J.* **2008**, *5*, 1–9.
15. The Biogas—Biogas Composition. Available online: https://www.biogas-renewable-energy.info/biogas_composition.html (accessed on 26 May 2026).
16. IEA Bioenergy. *A Perspective on the State of the Biogas Industry from Selected Member Countries*; IEA Bioenergy: Paris, France, 2022.
17. Hanum, F.; Yuan, L.; Kamahara, H.; et al. Treatment of Sewage Sludge Using Anaerobic Digestion in Malaysia: Current State and Challenges. *Front. Energy Res.* **2019**, *7*, 19. https://doi.org/10.3389/fenrg.2019.00019.
18. Xu, A.; Wu, Y.H.; Chen, Z.; et al. Towards the new era of wastewater treatment of China: Development history, current status, and future directions. *Water Cycle* **2020**, *1*, 80–87. https://doi.org/10.1016/j.watcyc.2020.06.004.
19. Chaubey, R.; Sahu, S.; James, O.O.; et al. A review on development of industrial processes and emerging techniques for production of hydrogen from renewable and sustainable sources. *Renew. Sustain. Energy Rev.* **2013**, *23*, 443–462. https://doi.org/10.1016/j.rser.2013.02.019.
20. Zhang, J.; Li, X.; Chen, H.; et al. Hydrogen production by catalytic methane decomposition: Carbon materials as catalysts or catalyst supports. *Int. J. Hydrogen Energy* **2017**, *42*, 19755–19775. https://doi.org/10.1016/j.ijhydene.2017.06.197.
21. Usman, M.; Daud, W.M.A.W.; Abbas, H.F. Dry reforming of methane: Influence of process parameters—A review. *Renew. Sustain. Energy Rev.* **2015**, *45*, 710–744. https://doi.org/10.1016/j.rser.2015.02.026.
22. Wittich, K.; Krämer, M.; Bottke, N.; et al. Catalytic Dry Reforming of Methane: Insights from Model Systems. *Chemcatchem* **2020**, *12*, 2130–2147. https://doi.org/10.1002/cctc.201902142.
23. Office of Fossil Energy, United States Department of Energy. *Hydrogen Production: Natural Gas Reforming*; Office of Fossil Energy, United States Department of Energy: Washington, DC, USA, 2020.

24. Zhang, J.; Wang, H.; Dalai, A.K. Development of stable bimetallic catalysts for carbon dioxide reforming of methane. *J. Catal.* **2007**, *249*, 300–310. https://doi.org/10.1016/j.jcat.2007.05.004.
25. Hao, Z.; Zhu, Q.; Jiang, Z.; et al. Characterization of aerogel Ni/Al_2O_3 catalysts and investigation on their stability for CH_4-CO_2 reforming in a fluidized bed. *Fuel Process. Technol.* **2009**, *90*, 113–121. https://doi.org/10.1016/j.fuproc.2008.08.004.
26. Hao, Z.; Zhu, Q.; Jiang, Z.; et al. Fluidization characteristics of aerogel Co/Al_2O_3 catalyst in a magnetic fluidized bed and its application to CH_4–CO_2 reforming. *Powder Technol.* **2008**, *183*, 46–52. https://doi.org/10.1016/j.powtec.2007.11.015.
27. Hua, W.; Jin, L.; He, X.; et al. Preparation of Ni/MgO catalyst for CO_2 reforming of methane by dielectric-barrier discharge plasma. *Catal. Commun.* **2010**, *11*, 968–972. https://doi.org/10.1016/j.catcom.2010.04.007.
28. Barroso-Quiroga, M.M.; Castro-Luna, A.E. Catalytic activity and effect of modifiers on Ni-based catalysts for the dry reforming of methane. *Int. J. Hydrogen Energy* **2010**, *35*, 6052–6056. https://doi.org/10.1016/j.ijhydene.2009.12.073.
29. Effendi, A.; Hellgardt, K.; Zhang, Z.G.; et al. Characterisation of carbon deposits on Ni/SiO_2 in the reforming of CH_4–CO_2 using fixed- and fluidised-bed reactors. *Catal. Commun.* **2003**, *4*, 203–207. https://doi.org/10.1016/S1566-7367(03)00034-7.
30. Huang, J.; Ma, R.; Huang, T.; et al. Carbon dioxide reforming of methane over Ni/Mo/SBA-15-La_2O_3 catalyst: Its characterization and catalytic performance. *J. Nat. Gas Chem.* **2011**, *20*, 465–470. https://doi.org/10.1016/S1003-9953(10)60226-5.
31. Zhu, J.; Peng, X.; Yao, L.; et al. Synthesis gas production from CO_2 reforming of methane over Ni–Ce/SiO_2 catalyst: The effect of calcination ambience. *Int. J. Hydrogen Energy* **2013**, *38*, 117–126. https://doi.org/10.1016/j.ijhydene.2012.07.136.
32. Yang, M.; Gao, W.; Zhang, H.; et al. Catalytic methane decomposition on an Fe-catalyst, coated on a novel fleece reactor. *Energy* **2025**, *335*, 138340. https://doi.org/10.1016/j.energy.2025.138340.
33. The Clean Hydrogen Ladder. Available online: https://www.liebreich.com/the-clean-hydrogen-ladder-now-updated-to-v4-1/ (accessed on 26 May 2026).
34. IEA. *The Role of E-Fuels in Decarbonising Transport*; IEA: Paris, France, 2023.
35. Hamedi, H.; Brinkmann, T.; Shishatskiy, S. Membrane-Assisted Methanol Synthesis Processes and the Required Permselectivity. *Membranes* **2021**, *11*, 596. https://doi.org/10.3390/membranes11080596.
36. Ye, J.; Dimitratos, N.; Rossi, L.M.; et al. Hydrogenation of CO_2 for sustainable fuel and chemical production. *Science* **2025**, *387*, 9388. https://doi.org/10.1126/science.adn9388.
37. Dang, S.; Li, M.; Gao, C.; et al. Size-dependent evolution of active-sites on Co_3O_4-modified In_2O_3 catalysts for CO_2 hydrogenation to methanol. *Appl. Catal. B Environ. Energy* **2026**, *395*, 126899. https://doi.org/10.1016/j.apcatb.2026.126899.
38. Guzman-Urbina, A.; Kitagawa, N.; Richards, D.; et al. Advancing e-methanol systems via direct air carbon capture, CO_2 hydrogenation, and hydrothermal co-electrolysis. *J. Clean. Prod.* **2025**, *528*, 146699. https://doi.org/10.1016/j.jclepro.2025.146699.
39. Beck, A.; Zabilskiy, M.; Newton, M.A.; et al. Following the structure of copper-zinc-alumina across the pressure gap in carbon dioxide hydrogenation. *Nat. Catal.* **2021**, *4*, 488–497. https://doi.org/10.1038/s41929-021-00625-x.
40. Jiang, Y.; Zhang, J.; Zhang, H.; et al. Green Methanol by Catalytic Multi-stage Fixed-bed Conversion of Biogas-based Syngas (CO, H_2). *SSRN* **2026**. https://doi.org/10.2139/ssrn.6670547.
41. Everaert, K.; Baeyens, J. Catalytic combustion of volatile organic compounds. *J. Hazard. Mater.* **2004**, *109*, 113–139. https://doi.org/10.1016/j.jhazmat.2004.03.019.
42. Hayes, R.; Kolaczkowski, S. *Introduction to Catalytic Combustion*; Routledge: London, UK, 2021. https://doi.org/10.1201/9780203750186.
43. Behrens, M.; Studt, F.; Kasatkin, I.; et al. The Active Site of Methanol Synthesis over Cu/ZnO/Al_2O_3 Industrial Catalysts. *Science* **2012**, *336*, 893–897. https://doi.org/10.1126/science.1219831.
44. Bennekom, J.; Winkelman, J.; Venderbosch, R.; et al. Modeling and Experimental Studies on Phase and Chemical Equilibria in High-Pressure Methanol Synthesis. *Ind. Eng. Chem. Res.* **2012**, *51*, 12233–12243. https://doi.org/10.1021/ie3017362.
45. Slotboom, Y.; Bos, M.; Pieper, J.; et al. Critical assessment of steady-state kinetic models for the synthesis of methanol over an industrial Cu/ZnO/Al_2O_3 catalyst. *Chem. Eng. J.* **2020**, *389*, 124181. https://doi.org/10.1016/j.cej.2020.124181.
46. Schagen, T.N.; Keestra, H.; Brilman, D.W.F. Improved kinetic model for methanol synthesis with Cu/ZnO/Al_2O_3 catalysts based on an extensive state-of-the-art dataset. *Chem. Eng. J.* **2025**, *507*, 159953. https://doi.org/10.1016/j.cej.2025.159953.
47. Graaf, G.H.; Scholtens, H.; Stamhuis, E.J.; et al. Intra-particle diffusion limitations in low-pressure methanol synthesis. *Chem. Eng. Sci.* **1990**, *45*, 773–783. https://doi.org/10.1016/0009-2509(90)85001-T.
48. UNIFAC Consortium at the Carl von Ossietzky University Oldenburg (Develops the PSRK Model Since 2005). Available online: https://unifac.ddbst.com/unifac_.html (accessed on 26 May 2026).

49. Parameters of the Original UNIFAC Model. Available online: https://www.ddbst.com/published-parameters-unifac.html (accessed on 26 May 2026).
50. Parameters of the Modified UNIFAC (Dortmund) Model. Available online: https://www.ddbst.com/PublishedParametersUNIFACDO.html (accessed on 26 May 2026).
51. Published Parameters of the PSRK Model. Available online: https://www.ddbst.com/psrk.html (accessed on 26 May 2026).
52. Horstmann, S.; Jabłoniec, A.; Krafczyk, J.; et al. PSRK group contribution equation of state: Comprehensive revision and extension IV, including critical constants and α-function parameters for 1000 components. *Fluid Phase Equilibria* **2005**, *227*, 157–164. https://doi.org/10.1016/j.fluid.2004.11.002.
53. Renon, H.; Prausnitz, J.M. Local compositions in thermodynamic excess functions for liquid mixtures. *AIChE J.* **1968**, *14*, 135–144. https://doi.org/10.1002/aic.690140124.
54. McDermott, C.; Ashton, N. Note on the definition of local composition. *Fluid. Phase Equilibria* **1977**, *1*, 33–35. https://doi.org/10.1016/0378-3812(77)80024-1.